Journal of Solid State Chemistry 297 (2021) 122058

Contents lists available at ScienceDirect

Journal of Solid State Chemistry

journal homepage: www.elsevier.com/locate/jssc

Off-stoichiometric semiconductors $Cu_{1.33+x}Zn_{1.33-x}In_{1.33}Se_4$ (x = 0, 0.1, 0.2 and 0.3): Synthesis, structure, and thermal and electrical properties

George S. Nolas [a,*], Hagen Poddig [a,b], Wencong Shi [a], Lilia M. Woods [a], Joshua Martin [c], Hsin Wang [d]

[a] Department of Physics, University of South Florida, Tampa, FL, 33620, USA
[b] Faculty of Chemistry and Food Chemistry, Technische Universität Dresden, 01062 Dresden, Germany
[c] Material Measurement Laboratory, National Institute of Standards and Technology, Gaithersburg, MD, 20899, USA
[d] Materials Science and Technology Division, Oak Ridge National Laboratory, Oak Ridge, TN, 37831, USA

A B S T R A C T

The synthesis, structure, and temperature dependent thermal and electrical properties of off-stoichiometric polycrystalline modified zinc blende quaternary chalcogenides $Cu_{1.33+x}Zn_{1.33-x}In_{1.33}Se_4$, where x = 0, 0.1, 0.2 and 0.3, are investigated. Temperature-dependent electrical properties reveal these compositions to be semiconductors with alteration of the carrier concentration and electrical transport via stoichiometric variation. The thermal conductivity is low for all specimens and intrinsic to these materials. First principles calculations are also reported in establishing a fundamental investigation that illustrates the large variation in stoichiometry that is possible in these materials. This stoichiometric variation results in the observed variation of the transport properties. The results presented reveal fundamental structure-property relationships in these quaternary chalcogenides, and provides a basis for further research into the viability for large stoichiometric variation in other materials that are of interest for technological applications.

1. Introduction

Quaternary chalcogenides can be composed of nontoxic, earth abundant elements and form in a variety of structure types [1–4]. For certain compositions and crystal structures tunable properties can be realized through stoichiometric changes leading to unique transport properties [5,6], and optimization for photovoltaic [4,7,8] or thermoelectric [9–12] applications. One class of quaternary chalcogenides can be represented as I-II_2-III-VI_4, where I = Cu or Ag, II = Zn, Cd or Hg, III = Al, Ga, In or Tl and VI = S, Se, or Te. This family of compounds is much less explored [13–16] than other quaternary chalcogenides. The formation of these stoichiometric multi-component systems can be considered as a result of atomic cross substitutions accompanied by lattice mutations in which the overall valence state is preserved, with charge neutrality in the periodic crystal [17,18].

Herein we report on the synthesis, crystal structure including first-principles calculations, and temperature dependent transport properties of modified zinc blende $Cu_{1.33+x}Zn_{1.33-x}In_{1.33}Se_4$ (x = 0, 0.1, 0.2, 0.3) quaternary chalcogenides for the first time. We investigate the effect of stoichiometric variations on the transport properties that, as described herein, can be exploited to dramatically vary the electrical properties. In addition, first principles calculations of the structural properties and formation energy of these quaternary chalcogenides are reported using density functional theory (DFT). This fundamental study is intended to provide an understanding of the effect of stochiometric variation on the transport properties of these materials, and gauge their suitability as materials for potential energy-related applications such as thermoelectrics or photovoltaics.

2. Experimental section

Modified zinc blende, or sphalerite-like, $Cu_{1.33}Zn_{1.33}In_{1.33}Se_4$ with space group $F\bar{4}3m$ was obtained when attempting to synthesize $CuZnInSe_3$ ($P\bar{4}2c$). In fact, we were unable to synthesize this latter composition that was reported to form in a chalcopyrite-like crystal structure [19]. It is clear that this chalcopyrite-like phase does not form by reaction of the elements as described herein. As described below, the crystal structure of $Cu_{1.33}Zn_{1.33}In_{1.33}Se_4$ is similar to that of $CuZn_2InSe_4$ [16], however, with excess Cu and In together with a deficiency in Zn. From this observation, we concluded that extreme off-stoichiometric compositions can be realized in these quaternary chalcogenides. We subsequently synthesized a series of compositions with increasing (decreasing) Cu (Zn) content, $Cu_{1.33+x}Zn_{1.33-x}In_{1.33}Se_4$ with x = 0.0, 0.1, 0.2 and 0.3, by elemental reaction of Cu powder (99.9%, Alfa Aesar), Zn powder

* Corresponding author.
E-mail address: gnolas@usf.edu (G.S. Nolas).

https://doi.org/10.1016/j.jssc.2021.122058
Received 13 November 2020; Received in revised form 3 February 2021; Accepted 9 February 2021
Available online 13 February 2021
0022-4596/© 2021 Elsevier Inc. All rights reserved.

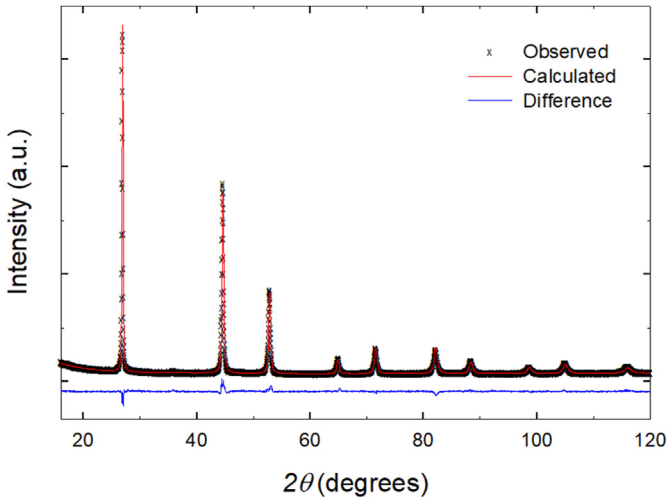

Fig. 1. Powder XRD data for $Cu_{1.33}Zn_{1.33}In_{1.33}Se_4$, including the profile fit and difference from Rietveld refinement.

Table 1
Rietveld refinement parameters for $Cu_{1.33}Zn_{1.33}In_{1.33}Se_4$.

Nominal Composition	$Cu_{1.33}Zn_{1.33}In_{1.33}Se_4$
Refined Composition	$Cu_{1.33}Zn_{1.33}In_{1.33}Se_4$
Space group	$F\bar{4}3m$ (*No.* 216)
Z	1
a(Å)	5.7503(1)
V (Å^3)	190.14(1)
Radiation	Graphite Monochromator CuK_α (1.54056 Å)
$D_{calc.}$ (g/cm^3)	5.596
2θ range (deg.)	16–120
Step width (deg)	0.025
wR_p, R_p	0.048, 0.037
Reduced χ^2	2.528

Table 2
Atomic coordinates and displacement parameters for $Cu_{1.33}Zn_{1.33}In_{1.33}Se_4$.

atoms	x (Å)	y (Å)	z (Å)	Uiso (Å^2)	occupancy
Cu	0.25	0.25	0.25	0.013(1)	1/3
Zn	0.25	0.25	0.25	0.013(1)	1/3
In	0.25	0.25	0.25	0.013(1)	1/3
Se	0	0	0	0.021(1)	1

(99.9%, Alfa Aesar), In chunks (99.9995%, Alfa Aesar) and Se powder (99.999%, Alfa Aesar) [20]. The elements were loaded into silica ampoules that were put into a quartz tube and evacuated to 0.13 Pa (10^{-3} Torr) before sealing. The elements were heated at a rate of 333 K per hour then reacted at 1363 K for 4 h before cooling to 848 K at a rate of 323 K per hour, and subsequently held at this temperature for 5 days. Following this reaction profile, the reaction tubes were allowed to naturally cool to room temperature. The specimens were then ground into fine powders (325 mesh: 44 μm), cold pressed into pellets, and sealed under vacuum for annealing at 673 K for 7 days. After annealing, the pellets were again ground into fine powders and sieved to 325 mesh before loading into a custom-designed tungsten carbide (WC) punch and die assembly for densification by spark plasma sintering (SPS) at 600 K and 400 MPa for 20 min under vacuum, resulting in dense pellets of ≥98% theoretical density. The high densities were obtained due to our WC tooling as higher pressures than typical for graphite tooling were realized. The WC die was lined with graphite foil to prevent reaction with the surrounding material.

Table 3
Formation energy, lattice constants, and average cation-anion distances calculated for the $CuZnInSe_3$ ($P\bar{4}2c$) and $CuZn_2InSe_4$ ($F\bar{4}3m$) structure types.

Nominal Composition	$CuZnInSe_3$	$CuZn_2InSe_4$
$\bar{E}_f$(eV)	−0.518	−0.570
a(Å)	5.831	5.804
b (Å)	5.829	5.804
c (Å)	11.682	11.624
$\bar{d}_{Cu-Se}$(Å)	2.441	2.436
$\bar{d}_{Zn-Se}$ (Å)	2.503	2.498
$\bar{d}_{In-Se}$ (Å)	2.647	2.634

The phase purity and structure were investigated by Rietveld refinement of powder x-ray diffraction (XRD) data collected by a Bruker D8 Focus Diffractometer in Bragg-Brentano geometry with Cu Kα radiation and a graphite monochromator. The stoichiometry and homogeneity were analyzed by Rietveld refinement using the Jana2006 software [21]. Energy dispersive X-ray spectroscopy (EDS) after SPS was performed on well-polished surfaces with an Oxford INCA X-Sight 7582 M (INCA software) equipped scanning electron microscope (SEM, JEOL JSM-6390LV), with data obtained from several random positions of the SPS pellet for each specimen.

The densified specimens were cut into 2 mm × 2 mm x 10 mm parallelepipeds using an abrasive slurry wire saw for high temperature Seebeck coefficient, S, and resistivity, ρ, measurements using an ULVAC ZEM-3 system with experimental uncertainty ($2u$, where u is the combined standard uncertainty component and 2 is the coverage factor) of ±5% and ±8% for S and ρ, respectively. High temperature thermal conductivity, κ, was determined using the equation $\kappa = D{\cdot}\alpha{\cdot}Cp$, where D is the measured density, α is the measured thermal diffusivity, and Cp is

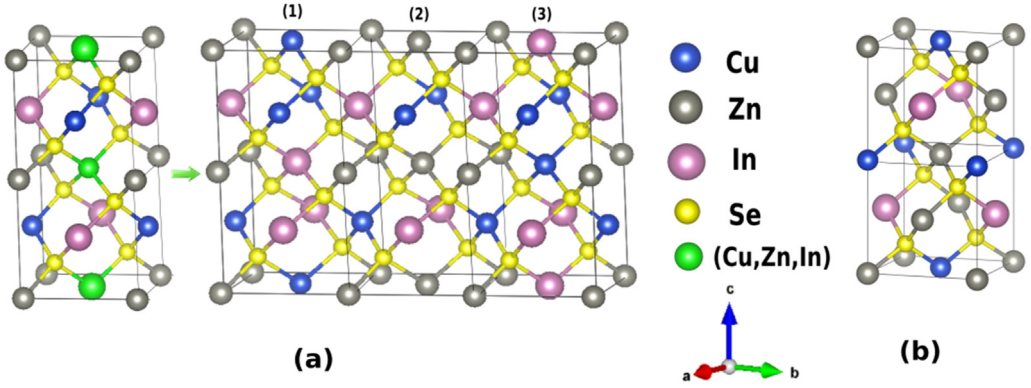

Fig. 2. Crystal structure for (a) $CuZnInSe_3$ in the modified chalcopyrite $P\bar{4}2c$ structure showing the standard unit cell as well as construction of the supercell consisting of three unit cells, as described in the text, and (b) $CuZn_2InSe_4$ in the modified zinc blende $F\bar{4}3m$ structure.

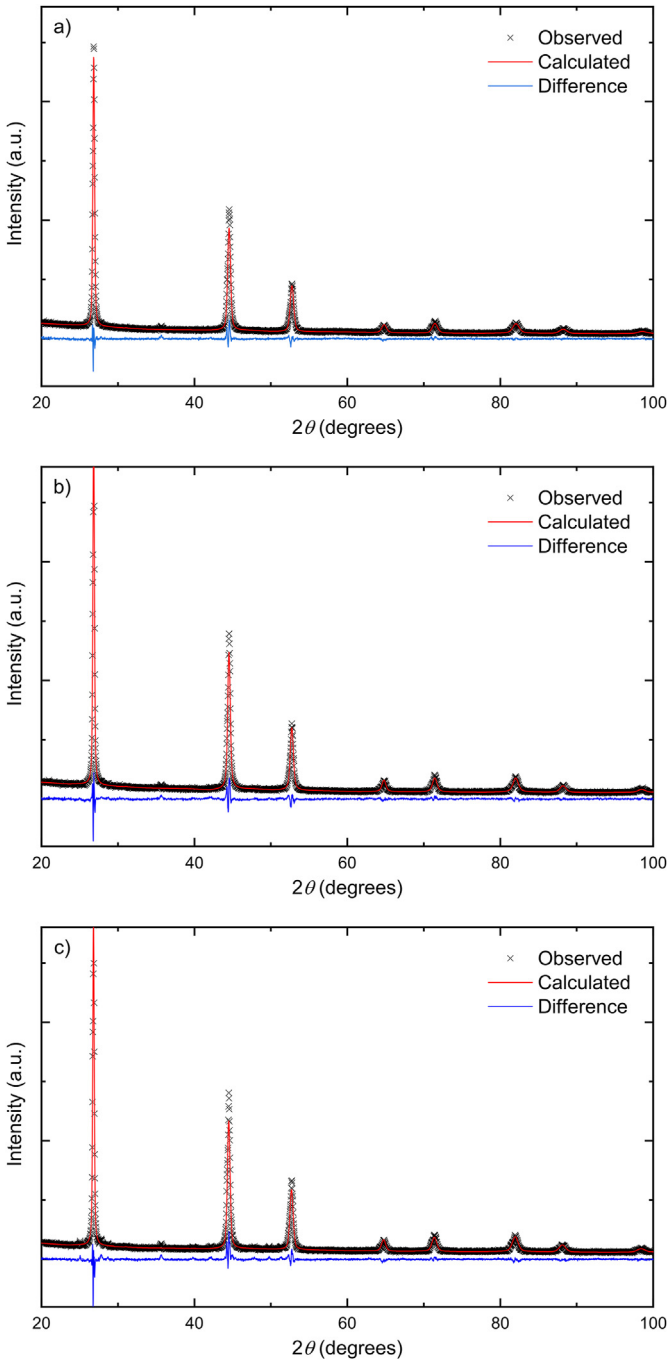

Fig. 3. Powder XRD data for (top) $Cu_{1.43}Zn_{1.23}In_{1.33}Se_4$, (middle) $Cu_{1.53}Zn_{1.13}In_{1.33}Se_4$ and (bottom) $Cu_{1.63}Zn_{1.03}In_{1.33}Se_4$, including the profile fit and difference from Rietveld refinement.

the specific heat. Thermal diffusivity was measured using the laser flash method in a flowing He environment with a NETZSCH LFA 457. The uncertainty ($2u$) in the thermal diffusivity measurements were ±5%. High temperature heat capacity Cp (≈Cv) was estimated with the Dulong-Petit limit (Cv = 3 nR, where n is the number of atoms per formula unit and R is the ideal gas constant). At high temperature, this may underestimate Cp; however, it is a good method for comparing the effect of doping and compositional changes since it eliminates the measurement uncertainties associated with heat capacity measurements [22]. Room temperature four-probe Hall measurements were collected in a magnetic field of up to 1 T, with the field alternating polarity to eliminate errors from voltage probe misalignment. The maximum experimental uncertainty ($2u$) in the Hall measurements were ±13%. A commercial Quantum Design Physical Property Measurement System was used for C_p measurements from 3 K to 250 K, where the experimental uncertainty ($2u$) of the measurement is less than ± 5% in the entire temperature range.

DFT calculations were performed with the *Vienna Ab initio Simulations Package* (VASP) based on the projector-augmented wave method that utilizes a plane wave basis set within periodic boundary conditions [23, 24]. The exchange correlation energy was included through the generalized gradient approximation (GGA) with the Perdew-Burke-Ernzerhof (PBE) functional. The convergence criteria for the relaxation process were 10^{-5} eV for total energy and 10^{-4} eVfor the force criteria. The energy cutoff was 384 eV and the tetrahedron integration methods with Bloechl corrections was utilized with 12 × 12 × 12 k-point mesh.

3. Results and Discussion

The Rietveld refinement results for $Cu_{1.33}Zn_{1.33}In_{1.33}Se_4$ are shown in Fig. 1 and Tables 1 and 2. The crystal structure of $Cu_{1.33}Zn_{1.33}In_{1.33}Se_4$ resembles a sphalerite-like structure with an equally-mixed cation site and Se on the anion site. Rietveld refinement of this structure was first performed with a chalcopyrite-like structure, as reported for CuMnMSe$_3$ (M = Al, Ga, In) [25] with space group $P\bar{4}2c$ and mixed cation sites. However, this model was rejected since additional reflections that should be present were not observed. Models based on related compounds, such as $CuInSe_2$ or $CuNiInSe_3$ that show idealized chalcopyrite structures with space group $I\bar{4}2d$ or $P\bar{4}2c$, respectively, would also require additional reflections [26, 27] that were non-compatible with our XRD results and were thus also rejected (note Figures S1 – S3 in the Supplemental Information). It is instructive to note K. Takei et al. [28] that report $I\bar{4}2d$ $CuInSe_2$ transitions to $F\bar{4}3m$ with addition of Zn. Therefore, in evaluating our data with these structure types we concluded that a statistically ordered cubic model with the metals equally occupying the cation site optimally described our data. This sphalerite-like structure contains a tetrahedral coordination of the metal cations by Se, with M–Se (M = Cu, Zn, In) distances of 2.4899(1) Å and a near ideal tetrahedral angle of 109.47(1)°.

In order to further study the properties of these materials, including the phase stability of the sphalerite-like structure as compared with other structure types, we performed DFT simulations to theoretically investigate the two main structure types described above, chalcopyrite $CuZnInSe_3$ and the modified zinc blende $Cu_{1.33}Zn_{1.33}In_{1.33}Se_4$. We note that because of computational limitations, calculations for $Cu_{1.33}Zn_{1.33}In_{1.33}Se_4$ are not possible since a very large supercell is needed to achieve the partial cation occupancy as obtained by our experiments, therefore, as a close prototype to the synthesized material we consider stoichiometric modified zinc blende $CuZn_2InSe_4$ theoretically [16]. In Fig. 2a we show the standard unit cell for $CuZnInSe_3$ in the chalcopyrite ($P\bar{4}2c$) crystal structure that includes 8 sites for the cations and 8 sites for the chalcogen anions. One of the atomic sites, the 2f Wyckoff position, is randomly occupied by the Cu, Zn, and In cations, therefore, in order to accommodate the three cations and achieve the correct elemental composition for $CuZnInSe_3$ a supercell of three unit cells (denoted as (1), (2) (3) in Fig. 2a), was constructed. We note that there are 24 cations to be accommodated in 24 atomic sites, however, the occupation ambiguity of the 2f Wyckoff position creates several possibilities for atomic arrangements. We explored several different possible arrangements and found that the lowest energy structure is achieved when the 2f Wyckoff positions in cell (1) is occupied by Cu and In, the 2f Wyckoff positions in cell (2) is occupied by Zn, and 2f Wyckoff positions in cell (3) is occupied by In and Cu, as shown in Fig. 2a. For the case of the $F\bar{4}3m$ space group, we again note that in order to accommodate the three types of cations in the 4a Wychoff positions, the atomic cell is constructed by placing vertically two-unit cells for the standard zinc blende structure, as shown in Fig. 2b. These two types of lattice structures were simulated using VASP within these relaxation criteria described in the previous section.

Table 4
Rietveld refinement parameters for the three additional compositions prepared for this study.

Nominal Composition	$Cu_{1.433}Zn_{1.233}In_{1.333}Se_4$	$Cu_{1.533}Zn_{1.133}In_{1.333}Se_4$	$Cu_{1.633}Zn_{1.033}In_{1.333}Se_4$
Refined Composition	$Cu_{1.433}Zn_{1.233}In_{1.333}Se_4$	$Cu_{1.533}Zn_{1.133}In_{1.333}Se_4$	$Cu_{1.633}Zn_{1.033}In_{1.333}Se_4$
Space group	$F\bar{4}3m$ (*No.* 216)	$F\bar{4}3m$ (*No.* 216)	$F\bar{4}3m$ (*No.* 216)
Z	1	1	1
a(Å)	5.7545(3)	5.7564 (1)	5.7551(3)
V ($Å^3$)	190.55(2)	190.74 (1)	190.61 (2)
Radiation	Graphite Monochromator CuK_α (1.54056 Å)		
$D_{calc.}$ (g/cm^3)	5.5821	5.5749	5.5771
2θ range (deg.)	20–100	20–100	20–100
Step width (deg.)	0.025	0.025	0.025
wR_p, R_p	0.068, 0.053	0.069, 0.054	0.074, 0.057
Reduced χ^2	2.016	2.496	2.958

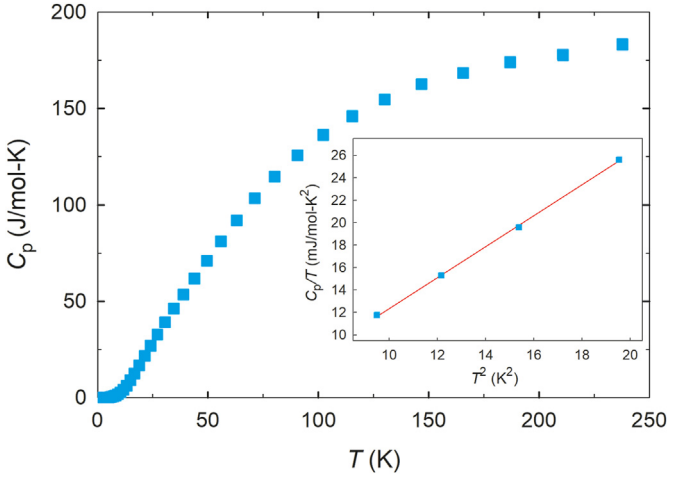

Fig. 4. Temperature-dependent C_p data for $Cu_{1.33}Zn_{1.33}In_{1.33}Se_4$, with the inset showing C_p/T vs T^2 at low temperatures and the solid line is a fit of the form $C_p/T = \gamma + \beta T^2$.

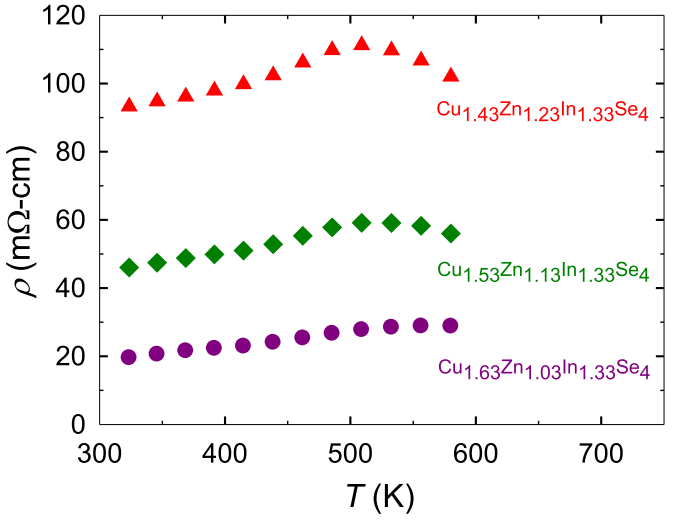

Fig. 5. Temperature dependent ρ for $Cu_{1.43}Zn_{1.23}In_{1.33}Se_4$ (red triangle), $Cu_{1.53}Zn_{1.13}In_{1.33}Se_4$ (green diamond) and $Cu_{1.63}Zn_{1.03}In_{1.33}Se_4$ (purple circle). (For interpretation of the references to colour in this figure legend, the reader is referred to the Web version of this article.)

The lattice constants a, b, c calculated for both systems after relaxation are given in Table 3, where we find that $a < b < c$ for the chalcopyrite structure and $a = b \approx c/2$ for the modified zinc blende material.

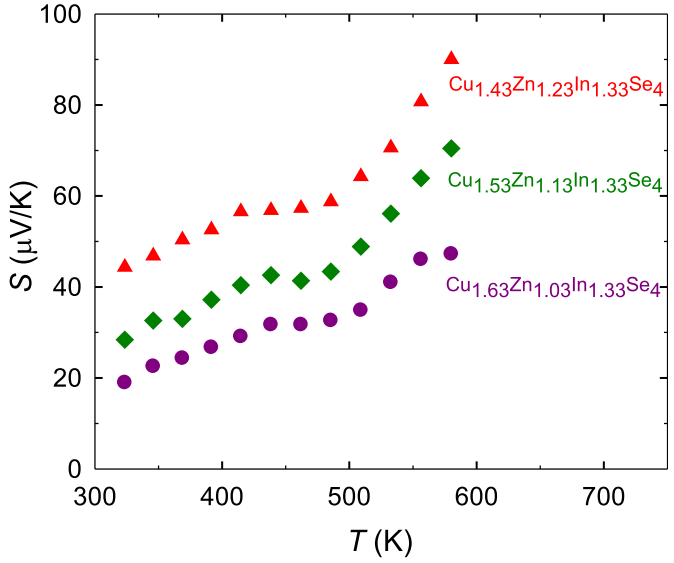

Fig. 6. Temperature dependent S for $Cu_{1.43}Zn_{1.23}In_{1.33}Se_4$ (red triangle), $Cu_{1.53}Zn_{1.13}In_{1.33}Se_4$ (green diamond) and $Cu_{1.63}Zn_{1.03}In_{1.33}Se_4$ (purple circle). (For interpretation of the references to colour in this figure legend, the reader is referred to the Web version of this article.)

The average cation-anion distances in both phases are also shown in Table 3. Both lattice parameters and average atomic distances are smaller for $CuZn_2InSe_4$ ($F\bar{4}3m$) as compared to $CuZnInSe_3$ ($P\bar{4}2c$), indicating better structural stability for the former compound. Moreover, the calculated lattice parameters and bond lengths are closer to our measured and refined values for the $F\bar{4}3m$ structure, whereas the model for $P\bar{4}2c$ has a larger deviation with our experimental data. To further shed light on the structural phase stability, we also calculated the average formation energy of both structure types according to $\overline{E}_f = \left(E_S - \sum_i n_i \overline{E}_i\right) \Big/ n$, where E_S is the total energy of the formed structure, n is the number of atoms in the unit cell, n_i is the number of ith type of atom in each cell, and $\overline{E}_i$ is the average energy of ith atom in its pure atomic phase. Our results show that $\overline{E}_f$ for the $CuZn_2InSe_4$ has a lower energy compared to $CuZnInSe_3$, giving strong corroborating evidence in support of our experimental findings for the assigned structure type.

Based on all these results, we synthesized compositions with increasing stoichiometric variation. Fig. 3 shows the Rietveld refinement results for the three additional compositions synthesized in order to investigate the change in transport properties with stoichiometric variation, with the refinement results shown in Table 4. The stoichiometries were confirmed by our EDS data.

The C_p data from 3 to 250 K for $Cu_{1.33}Zn_{1.33}In_{1.33}Se_4$ are shown in Fig. 4. The inset in Fig. 4 shows C_p/T versus T^2 data below 6 K. The solid

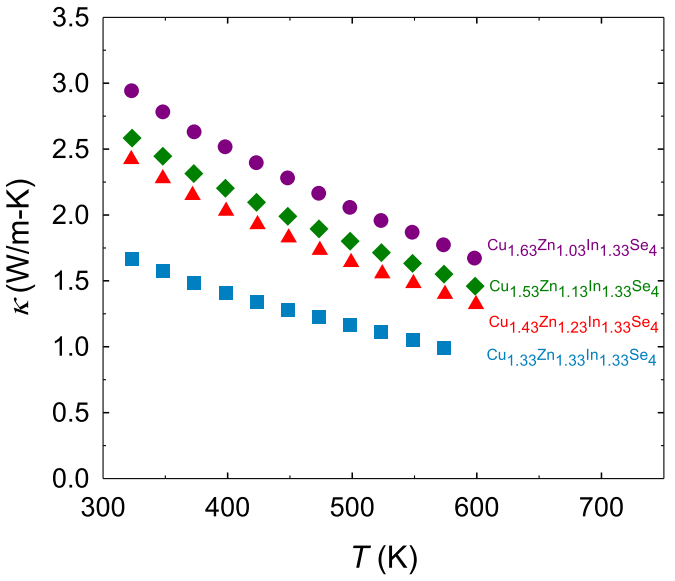

Fig. 7. Temperature dependent κ for $Cu_{1.33}Zn_{1.33}In_{1.33}Se_4$ (blue squares), $Cu_{1.43}Zn_{1.23}In_{1.33}Se_4$ (red triangle), $Cu_{1.53}Zn_{1.13}$ $In_{1.33}Se_4$ (green diamond) and $Cu_{1.63}Zn_{1.03}In_{1.33}Se_4$ (purple circle). (For interpretation of the references to colour in this figure legend, the reader is referred to the Web version of this article.)

line in the inset is a fit to the data of the form $C_p/T = \gamma+\beta T^2$, where γ is the Sommerfeld coefficient of the electronic contribution to the specific heat and β is the coefficient of the lattice contribution. Using this fit and employing the relation [29].

$$\theta_D = \left(\frac{12\pi^4 R n_a}{5\beta}\right)^{1/3} \quad (1)$$

where R is the molar gas constant and n_a is the number of atoms per formula unit, we estimate the Debye temperature, θ_D, to be 223 K and $\gamma = -0.001$ J mol^{-1} K^{-2}. The Sommerfeld coefficient, basically a null value, indicates a very low density of states at the Fermi level, which is reasonable given the very high resistivity for this composition.

Temperature dependent ρ measurements for $Cu_{1.33+x}Zn_{1.33-x}In_{1.33}Se_4$ for x = 0.1, 0.2 and 0.3 are shown in Fig. 5. The high electrical resistance for $Cu_{1.33}Zn_{1.33}In_{1.33}Se_4$ prevented ρ and S measurements on this composition. As shown in Fig. 5, ρ decreases with increasing stoichiometric variation. This is directly related to the change in carrier concentration that increases (decreases) with increasing (decreasing) Cu (Zn) content. Furthermore, ρ increases slightly with increasing temperature, indicative of degenerate semiconductor behavior. From our Hall measurements, holes are the majority carriers, with room temperature hole concentrations, p, of 1.1×10^{20}/cm^3, 4.7×10^{20}/cm^3 and 8.2×10^{20}/cm^3 for the x = 0.1, 0.2 and 0.3 specimens, respectively. Fig. 6 shows the measured S values for the three specimens. The S values correspond with the ρ data shown in Fig. 5, decreasing with increasing (decreasing) Cu (Zn) content and carrier concentration. The positive S values for all specimens implies p-type conduction and corroborates the Hall data.

For a single parabolic band model, S and p are given by Ref. [30].

$$S = \frac{k_B}{e}\left(\frac{(2+r)F_{1+r}(\eta)}{(1+r)F_r(\eta)} - \eta\right) \quad (2)$$

and

$$p = \frac{4\pi(2m_e k_B T)^{3/2}}{h^3}\left(\frac{m^*}{m_e}\right)^{3/2} F_{1/2}(\eta) \quad (3)$$

where r is the exponent of the energy dependence of the electron mean free path, η (= E_F/k_BT) is the reduced Fermi energy, E_F is the Fermi energy, F_r is the Fermi integral of order r [31,32], m^* is the hole effective mass, m_e is the free electron mass, and h is the Planck constant. For ionized impurity scattering $r = 2$ and for lattice vibrations $r = 0$. In this study we used the intermediate value $r = 1$. From our room temperature S and p values, we obtain $m^* = 0.2\ m_e$ for $Cu_{1.43}Zn_{1.23}In_{1.33}Se_4$ and $m^* = 0.4\ m_e$ for $Cu_{1.53}Zn_{1.13}In_{1.33}Se_4$ and $Cu_{1.63}Zn_{1.03}In_{1.33}Se_4$. These m* values are in agreement with previous reports on other quaternary chalcogenide material systems [14,16,33].

Fig. 7 shows the κ values for all four compositions. These κ values are primarily due to the lattice contribution, κ_L, of κ as estimated using the Wiedemann-Franz relation $\kappa = \kappa_E + \kappa_L$, where $\kappa_E = L_0 T/\rho$ (with Lorenz number, L_0, taken to be 2.44×10^{-8} V^2/K^2). Accordingly, $\kappa \approx \kappa_L$ for all specimens with a small increase with increasing Cu content. The κ values for all specimens are relatively low, with κ decreasing with increasing temperature, and in the same range as current and potential new materials optimized for thermoelectric applications [34–38].

4. Conclusion

The crystal structure, electrical transport and thermal properties of p-type off-stoichiometric zinc-blende-type quaternary chalcogenides are reported. The high resistivity of $Cu_{1.33}Zn_{1.33}In_{1.33}Se_4$ is on par with that of $CuZn_2InSe_4$ [16], however, the electrical properties can be dramatically altered with stoichiometric change. In fact, our results point to an insulating to semiconducting changeover in electronic transport with stoichiometry. Hole concentration and the electrical properties are varied with stoichiometric variation, while κ remains low. Although the thermoelectric figure of merit [34], $ZT = (S^2/\rho\kappa)T$, is low for these unoptimized compositions, our findings illustrate the extent and degree of stoichiometric variation that can be realized in these quaternary chalcogenides. Similar variation in stoichiometry may be attainable in other quaternary chalcogenides with different structure types, and can presumably also result in large variation in their electrical properties. This would be an interesting avenue to explore for other chalcogenide material systems.

CRediT authorship contribution statement

George S. Nolas: Conceptualization, Writing - original draft, Writing - review & editing, Project administration. **Hagen Poddig:** Formal analysis, Visualization. **Wencong Shi:** Formal analysis, Visualization. **Lilia M. Woods:** Formal analysis. **Joshua Martin:** Investigation. **Hsin Wang:** Investigation.

Declaration of competing interest

The authors declare that they have no known competing financial interests or personal relationships that could have appeared to influence the work reported in this paper.

Acknowledgments

This work was supported by National Science Foundation Grant No. DMR-1748188. H.P. acknowledges support by the ERASMUS + ICM WORLDWIDE exchange program funded by the European Union. We thank N. Alzahrani for sample preparation and Hall measurements, and W.D.C.B. Gunatilleke for XRD data and analyses. H.W. acknowledges support of the International Energy Agency (IEA) Advanced Materials for Transportation and the Department of Energy Lightweight and Propulsion Materials program under the Vehicle Technologies Office. Oak Ridge National Laboratory is managed by UT-Battelle LLC under contract DE-AC05000OR22725.

Appendix B. Supplementary data

Supplementary data related to this article can be found at https://doi.org/10.1016/j.jssc.2021.122058.

References

[1] X. Li, D. Zhuang, N. Zhang, M. Zhao, X. Yu, P. Liu, Y. Wei, G. Ren, J. Mater. Chem. 7 (2019) 9948–9957.
[2] Y. Dong, A.R. Khabibullin, K. Wei, J.R. Salvador, G.S. Nolas, L.M. Woods, ChemPhysChem 16 (2015) 3264–3270.
[3] Y. Dong, A.R. Khabibullin, K. Wei, Z.-H. Ge, J. Martin, J.R. Salvador, L.M. Woods, G.S. Nolas, Appl. Phys. Lett. 104 (2014) 252107.
[4] S. Chen, A. Walsh, X.G. Gong, S.H. Wei, Adv. Mater. 25 (2013) 1522–1539.
[5] K. Wei, G.S. Nolas, ACS Appl. Mater. Interfaces 7 (2015) 9752–9757.
[6] K. Wei, A.R. Khabibullin, T. Stedman, L.M. Woods, G.S. Nolas, J. Appl. Phys. 122 (2017) 105109.
[7] T.K. Todorov, J. Tang, S. Bag, O. Gunawan, T. Gokmen, Y. Zhu, D.B. Mitzi, Adv. Energy Mater. 3 (2013) 34–38.
[8] W. Wang, M.T. Winkler, O. Gunawan, T. Gokmen, T.K. Todorov, Y. Zhu, D.B. Mitzi, Adv. Energy Mater. 4 (2014) 1301465.
[9] M.L. Liu, I.W. Chen, F.Q. Huang, L.D. Chen, Adv. Mater. 21 (2009) 3808–3812.
[10] W.G. Zeier, Y. Pei, G. Pomrehn, T. Day, N. Heinz, C.P. Heinrich, G.J. Snyder, W. Tremel, J. Am. Chem. Soc. 135 (2013) 726–732.
[11] M. Ibáñez, R. Zamani, A. LaLonde, D. Cadavid, W. Li, A. Shavel, J. Arbiol, J.R. Morante, S. Gorsse, G.J. Snyder, A. Cabot, J. Am. Chem. Soc. 134 (2012) 4060–4063.
[12] Y. Dong, H. Wang, G.S. Nolas, Phys. Status Solidi RRL 8 (2014) 61–64.
[13] W. Shi, A.R. Khabibullin, D. Hobbis, G.S. Nolas, L.M. Woods, J. Appl. Phys. 125 (2019) 155101.
[14] D. Hobbis, W. Shi, A. Popescu, K. Wei, R.E. Baumbach, H. Wang, L.M. Woods, G.S. Nolas, Dalton Trans. 49 (2020) 2273–2279.
[15] D. Hobbis, K. Wei, H. Wang, G.S. Nolas, J. Alloys Compd. 743 (2018) 543–546.
[16] G.S. Nolas, M.S. Hassan, Y. Dong, J. Martin, J. Solid State Chem. 242 (2016) 50–54.
[17] B.R. Pamplin, J. Phys. Chem. Solid. 25 (1964) 675–684.
[18] W. Shi, A.R. Khabibullin, L.M. Woods, Adv. Theory and Simul. (2020) 2000041.
[19] G.E. Delgado, P. Grima-Gallardo, M. Quintero, Rev. Mexic. Fisica 62 (2016) 393–397.
[20] Certain commercial equipment, instrumentation, or materials are identified in this document. Such identification does not imply recommendation or endorsement by the National Institute of Standards and Technology, nor does it imply that the products identified are necessarily the best available for the purpose.
[21] V. Petrícek, M. Dušek, L. Palatinus, Z. für Kristallogr. - Cryst. Mater. 229 (2014) 345–352.
[22] H. Wang, W.D. Porter, H. Böttner, J. König, L. Chen, S. Bai, T.M. Tritt, A. Mayolet, J. Senawiratne, C. Smith, F. Harris, P. Gilbert, J. Sharp, J. Lo, H. Kleinke, L. Kiss, J. Electron. Mater. 42 (2013) 1073–1084.
[23] G. Kresse, J. Furthmüller, Comput. Mater. Sci. 6 (1996) 15–50.
[24] G. Kresse, J. Furthmüller, Phys. Rev. B 54 (1996) 11169–11186.
[25] G.E. Delgado, J.A. Flores-Cruz, P. Grima-Gallardo, M. Quintero, A. Moreno, Mater. Res. 21 (2018) 3–8.
[26] K.S. Knight, Mater. Res. Bull. 27 (1992) 161–167.
[27] J.M. Merino, J.L. Martín De Vidales, S. Mahanty, R. Díaz, F. Rueda, M. León, J. Appl. Phys. 80 (1996) 5610–5616.
[28] K. Takei, T. Maeda, F. Gao, S. Yamazoe, T. Wada, Jpn. J. Appl. Phys. 53 (2014), 05FW07-1-6.
[29] J.M. Ziman, Principles of the Theroy of Solids, Cambridge University Press, Cambridge, 1964.
[30] G.A. Slack, M.A. Hussain, J. Appl. Phys. 70 (1991) 2694–2718.
[31] P. Rhodes, Proc. Roy. Soc. Lond. A204 (1950) 396–405.
[32] J. McDougall, E.C. Stoner, Phil. Trans. Roy. Soc. Lond. A237 (1938) 67–104.
[33] K. Wei, L. Beauchemin, H. Wang, W.D. Porter, J. Martin, G.S. Nolas, J. Alloys Compd. 650 (2015) 844–847.
[34] G.S. Nolas, J.W. Sharp, H.J. Goldsmid, Thermoelectric: Basics Principles and New Materials Developments, Springer-Verlag, Berlin, 2001.
[35] A. Datta, J. Paul, A. Kar, A. Patra, Z. Sun, L. Chen, J. Martin, G.S. Nolas, Cryst. Growth Des. 10 (2010) 3983–3989.
[36] G.S. Nolas, G.A. Slack, Am. Sci. 89 (2001) 136–141.
[37] G. Tan, Z. Li-Dong, M.G. Kanatzidis, Chem. Rev. 116 (2016) 12123–12149.
[38] L. Yang, Z.G. Chen, M.S. Dargusch, J. Zou, Adv. Energy Mater. 8 (2018) 1701797.